Performance Analysis of a Countercurrent Flow Heat Exchanger Placed on the Truck Compartment Roof

Lin, Wamei; Yuan, Jinliang; Sundén, Bengt

Published in:
Journal of Thermal Science and Engineering Apllications

DOI:
10.1115/1.4007438

2012

Performance Analysis of a Countercurrent Flow Heat Exchanger Placed on the Truck Compartment Roof

Wamei Lin

Jinliang Yuan

Bengt Sundén[1]

e-mail: bengt.sunden@energy.lth.se

Department of Energy Sciences,
Lund University,
P. O. Box 118,
S-221 00 Lund, Sweden

Due to the increasing power requirement and the limited available space in vehicles, placing the heat exchanger at the roof or the underbody of vehicles might increase the possibility to handle the cooling requirement. A new configuration of the heat exchanger has to be developed to accommodate with the position change. In this paper, a countercurrent heat exchanger is developed for position on the roof of the vehicle compartment. In order to find an appropriate configuration of fins with high thermal performance on the air side, the computational fluid dynamics approach is applied for a comparative study among louver fin, wavy fin, and pin fin by using ANSYS FLUENT software. It is found that the louver fin performs high thermal performance and low pressure drop. Thus, the louver fin is chosen to be the configuration of the countercurrent flow heat exchanger. It is also found that the countercurrent flow heat exchanger presents higher heat transfer coefficient than the cross flow heat exchanger. Furthermore, the overall size and the air pumping power of the countercurrent flow heat exchanger are lower than those in the cross flow heat exchanger. Several suggestions and recommendations are highlighted. [DOI: 10.1115/1.4007438]

Keywords: thermal performance, pressure drop, countercurrent flow, heat exchanger, roof of vehicles

1 Introduction

Low fuel consumption, low carbon dioxide emission, and low noise emission become much more important than before in the vehicle industry. These requirements lead to a number of technical developments, e.g., new concept on primary missions control like homogeneous charge compression ignition engines, after treatment like exhaust gas recirculation valves [1], and noise shields within the engine compartment. All these efforts increase the operating temperature in the engine compartment. In order to keep the engine working at its optimal conditions, a huge amount of heat has to be released from the engine to the ambient. In modern heavy vehicles, this heat is so huge that a conventional heat exchanger (HEX) cannot handle it easily. In addition, more and more electric powertrain is introduced to heavy vehicles. Because the operating temperature of electric equipment (battery: $\sim$55 °C) is much lower than that of a combustion engine (combustion engine: $\sim$90 °C) [2], larger cooling surface area has to be used for the battery cooling than the one for the combustion engine cooling. However, there is space limitation in vehicles. It is impossible to increase the size of the radiator to dissipate the huge amount of heat from the vehicle. All these factors lead to a revolution of the radiator design in vehicles.

An idea of new HEXs suggested some time ago is to place HEXs at the underbody of vehicles [3–5]. For instance, most public buses have the engine radiator at the underbody. This is mostly due to the engine position (at the rear of the bus). Recently, the Centro Ricerche Fiat [5] used some parts of the vehicle body panels as HEXs to reduce the radiator size in light duty vehicles. Two roll bond HEXs were installed on the engine hood and below the engine, respectively. These could dissipate 60% of heat from the engine for all the test conditions. In addition, two levels of cooling systems (high temperature and low temperature systems) were introduced to a car in Ref. [6]. The condenser and the intercooler were cooled by liquid instead of air. Thus, the condenser and the intercooler could be relocated from the front of the vehicle to other more suitable places. The rearrangement of HEXs position led to 4% reduction of fuel consumption in the vehicle. Previous studies have shown that the cooling power could be increased and the fuel consumption would be reduced by rearranging the position of HEXs in vehicles [4].

The conventional radiator of the heavy duty vehicles is placed in the front of the vehicle, as shown in Fig. 1. A possible position for placing the radiator is the roof of driver compartment. If the radiator is placed on the roof (as shown in Fig. 1), the coolant flow direction and the air flow direction would be opposite. This is typical principle of a countercurrent flow HEX [7]. However, the engine radiator is normally a cross flow HEX in vehicles. Based on the HEX design theory, generally a countercurrent flow HEX has better thermal performance than does a cross flow HEX, see Ref. [7]. Thus, the option of placing a countercurrent flow HEX on the roof of the truck driver compartment might be a good idea to the engine radiator revolution.

In order to evaluate the performance of the countercurrent flow HEX on the roof of the truck driver compartment, various configurations of fins in HEX are evaluated to choose an appropriate one in this paper. Based on Ref. [8], three configurations of fins (louver-, wavy-, and pin fin) are adopted and analyzed by the ANSYS FLUENT software on the air side of a countercurrent flow HEX. The one presenting high thermal performance and low pressure drop will be selected to compare with a conventional cross flow HEX (louver fin is on the air side and flat tube on the

[1]Corresponding author.

Manuscript received January 17, 2012; final manuscript received June 22, 2012; published online October 12, 2012. Assoc. Editor: Arun Muley.

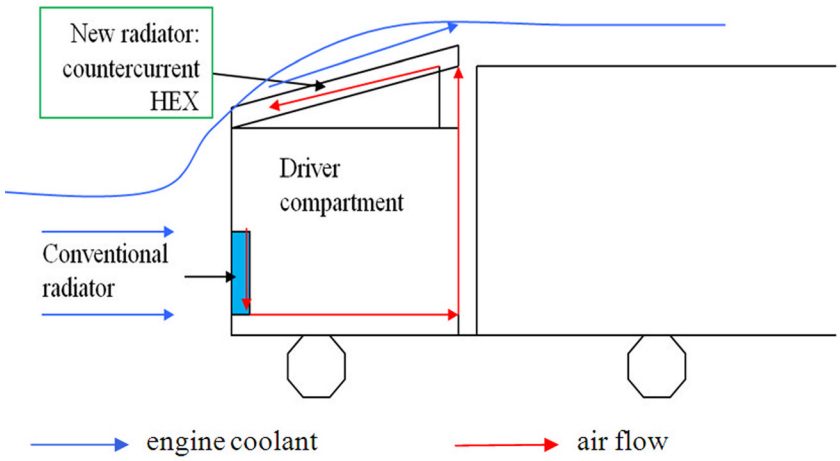

Fig. 1 Schematics of the positions of a radiator in trucks

water side), in terms of thermal performance. Several advantages and disadvantages of the countercurrent flow HEX are outlined and discussed based on a specific case study at the end of the paper.

2 Description of Physical Model and Assumptions

A simplified model of the countercurrent flow HEX is shown in Fig. 2. The engine coolant flows in the negative direction of x-axis. However, the air flow direction (the positive direction of x-axis) is opposite to the direction of engine coolant, as shown in Fig. 2(*a*). Three different configurations of fins (louver-, wavy-, and pin fin) are placed on the air side of HEX, as shown in Figs. 2(*b*)–2(*d*), respectively. The fluid is assumed to be incompressible with constant properties and in steady-state. The engine coolant is assumed to be water. The countercurrent flow HEX is made of aluminum. The thermal resistance between the water tubes and the fins is neglected. In order to simplify the simulation model and save computational time, only a core of the HEX is adopted, as shown in Fig. 2. The overall size of the core is 2.31 mm × 6.85 mm × 70.00 mm (W × H × L). The parameters of the fins are presented in Table 1.

3 Mathematical Formulation and Numerical Method

3.1 Adoption of Flow Model. Based on the European law, the maximum velocity of heavy vehicles is 80 km/h. Thus, the air inlet velocity in the simulation is ranging from 50 to 70 km/h. In this case, the Reynolds number on the air side is from 2400 to 5000. Thus, low Reynolds number turbulent flow prevails on the air side. In order to capture the low Reynolds number turbulent flow, the "renormalization group" (RNG) k-ε turbulence model is adopted [9,10]. However, laminar flow is used on the water side, in order to simplify the simulation model (the inlet velocity of water is assumed to be less than 2 m/s).

3.2 Governing Equations. The governing equations for continuity, momentum, and energy can be expressed as follows [11]:

Continuity equation

$$\frac{\partial(\rho u_i)}{\partial x_i} = 0 \tag{1}$$

Momentum equations

$$\frac{\partial(\rho u_i u_j)}{\partial x_j} = -\frac{\partial p}{\partial x_i} + \frac{\partial}{\partial x_j}\left((\mu + \delta\mu_t)\left(\frac{\partial u_i}{\partial x_j} + \frac{\partial u_j}{\partial x_i}\right)\right) \tag{2}$$

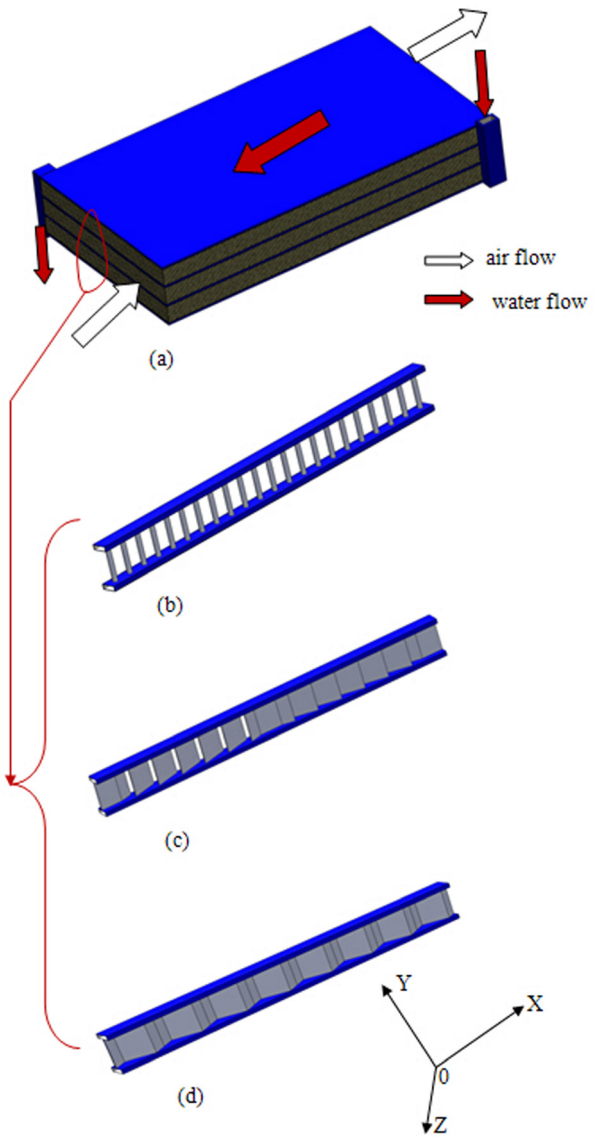

Fig. 2 (*a*) Schematics of the countercurrent flow HEX, with (*b*) louver, (*c*) wavy, and (*d*) pin fin core

Table 1 Parameters of louver fin, wavy fin, and pin fin (mm)

Louver fin [8]	Fin pitch 2.31	Fin thickness 0.152	Louver spacing 4.76	Louver angle (deg) 17.06
Wavy fin	Fin pitch 2.23	Fin thickness 0.152	Wave length 8.9	Wave amplitude 1
Pin fin	Pin pattern In-line	Pin diameter 0.79	Transverse spacing 2.3	Longitudinal spacing 3.18

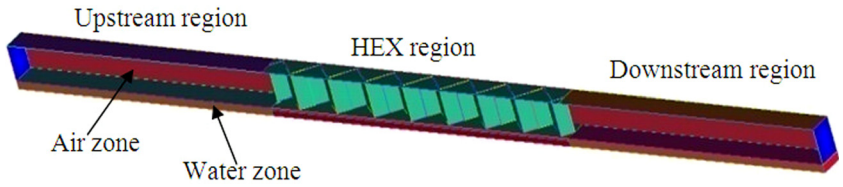

Fig. 3 Computational domain

Energy equation

$$\frac{\partial(\rho\mu_j T)}{\partial x_j} = \frac{\partial}{\partial x_j}\left(\left(\frac{\mu}{Pr} + \delta\frac{\mu_t}{Pr_t}\right)\frac{\partial T}{\partial x_j}\right) \tag{3}$$

When laminar flow (the water side) prevails, $\delta = 0$; when turbulent flow (the air side) prevails, $\delta = 1$. The equations of turbulent kinetic energy k and the rate of energy dissipation ε corresponding to the RNG k-ε turbulence model are

Turbulent kinetic energy k equation

$$\frac{\partial}{\partial x_i}(\rho k u_i) = \frac{\partial}{\partial x_j}\left(\left(\mu + \frac{\mu_t}{\sigma_k}\right)\frac{\partial k}{\partial x_j}\right) + P_k - \rho\varepsilon \tag{4}$$

Rate of energy dissipation ε equation

$$\frac{\partial}{\partial x_i}(\rho\varepsilon u_i) = \frac{\partial}{\partial x_j}\left(\left(\mu + \frac{\mu_t}{\sigma_\varepsilon}\right)\frac{\partial \varepsilon}{\partial x_j}\right) + C_{1s}\frac{\varepsilon}{k}p_k - C_{2s}^*\rho\frac{\varepsilon^2}{k} \tag{5}$$

where

$$C_{2s}^* = C_{2s} + \frac{c_\mu\eta^3(1-\eta/\eta_0)}{1+\beta\eta^3}, \quad \mu_t = \rho C_\mu\frac{k^2}{s},$$
$$\eta = sk/\varepsilon, \quad \text{and} \quad s = (2s_{ij}s_{ij})^{1/2}$$

The values of all of the constants are as follows (see Ref. [12]):

$$C_\mu = 0.0845; \quad \sigma_k = 0.7194; \quad \sigma_\varepsilon = 0.7194;$$
$$C_{\varepsilon 1} = 1.42; \quad C_{\varepsilon 2} = 1.68; \quad \eta_0 = 4.38; \quad \beta = 0.012$$

3.3 Computational Domain and Boundary Conditions. The louver-, wavy-, and pin fins are symmetrical in the height direction. Thus, only half of the fin height is simulated. The water tube is also simulated by using half height. On the other hand, in order to eliminate the effect of the entrance, the computational domain is extended upstream by an additional length of the HEX. Meanwhile, the computational domain is also extended downstream with the length of the HEX to eliminate the effect of outlet on the flow inside the HEX. Thus, the whole length of the computational domain is three times of the length of the HEX, as shown in Fig. 3.

Because there are air and water zones in the simulation, the boundary conditions should be specified in different zones separately.

1. Air zone
   (a) Upstream region: top-, front-, and back sides are symmetry surfaces; left side is the velocity inlet.
   (b) Downstream region: top-, front-, and back sides are symmetry surfaces; right side is the outlet.
   (c) HEX region: top side is symmetry surface; front side and back side are periodic (as the geometry of louver fin or wavy fin is not symmetry).
2. Water zone
   (a) Upstream region: bottom-, front-, and back sides are symmetry surfaces; left side is the outlet.
   (b) Downstream region: bottom-, front-, and back sides are symmetry surfaces; right side is the velocity inlet (the temperature difference between the air inlet and the water inlet is set to 50 °C).
   (c) HEX region: bottom-, front-, and back sides are symmetry surfaces.

3.4 Numerical Method. The commercial code ANSYS FLUENT 12.0 is used for the numerical solution. A finite volume method is adopted to convert the governing equations to algebraic equations so that they can be solved numerically [12]. The SIMPLE algorithm is used to couple pressure and velocity. A second-order upwind scheme is introduced to the space discretization of the momentum, energy, and turbulence equations in the simulations. The convergence criterion for continuity, momentum, k, and ε equations is below 10^{-3}. However, in order to ensure an energy balance between the water zone and the air zone under the countercurrent flow condition, the convergence criterion of energy is below 10^{-8}.

The mesh generation is carried out by the ICEM software. In order to check the grid independence, three sets of mesh size (coarse: $20 \times 28 \times 250$; middle: $22 \times 34 \times 340$; fine: $26 \times 38 \times 368$) are chosen to be compared in the wavy fin (HEX region in the air zone). The predicted pressure drop and Nusselt number from these three sets of mesh are shown in Table 2. It is found that the deviation of the pressure drop and Nusselt number between the middle case and the fine case is 2.5% and 4.6%, respectively. In order to save computational time and keep the accuracy of the simulation, the middle mesh size ($22 \times 34 \times 340$) is chosen for the wavy fin. The same method was also adopted to check the grid independence of the louver fin and the pin fin.

4 Results and Discussion

4.1 Parameter Definitions. Before analyzing and comparing the fluid flow and heat transfer characteristics for three different configurations of countercurrent flow HEX (louver-, wavy-, and pin fin), the definitions of Nusselt (Nu) number, Stanton (St) number, and friction factor (f) are presented. First, the Nusselt number and Stanton number are calculated as

Table 2 Grid independence study for wavy fin (Re = 3700)

	Coarse ($20 \times 28 \times 250$)	Middle ($22 \times 34 \times 340$)	Fine ($26 \times 38 \times 368$)
△P (Pa)	1350 (19%)	1155 (2.5%)	1126 (base)
Nu	34.2 (54.5%)	23.16 (4.6%)	22.13 (base)

Table 3 Deviation between the simulation model and the experiment

Re	$StPr^{2/3}$ in Ref. [8]	Simulation $StPr^{2/3}$	f in Ref. [8]	Simulation f
2837	0.0092	0.0097 (5.4%)	0.0435	0.044 (1.1%)
3392	0.0087	0.0086 (1.2%)	0.041	0.04 (2.4%)
3769	0.0082	0.0081 (1.2%)	0.0398	0.0382 (4.1%)

$$Re = \frac{\rho_f \cdot u_{\max} \cdot D_h}{\mu} \tag{6}$$

$$h_f = \frac{Q}{A_0 \Delta T} \tag{7}$$

$$Nu = h_f \cdot \frac{D_h}{\lambda_f} \tag{8}$$

$$St = \frac{h_f}{\rho_f \cdot u_{\max} \cdot C_p} \tag{9}$$

where, Q is the total amount of heat dissipated to air (W), A_0 the fin surface area (m^2), △T the logarithmic mean temperature difference, i.e., LMTD (K) and D_h the hydraulic diameter (m). These are defined as follows:

$$Q = m \cdot c_p \cdot (T_{\text{out}} - T_{\text{in}}) \tag{10}$$

$$\Delta T = \frac{(\Delta T_{\max} - \Delta T_{\min})}{ln \dfrac{\Delta T_{\max}}{\Delta T_{\min}}} \tag{11}$$

$$\Delta T_{\max} = \max(T'_{\text{out}} - T_{\text{in}}, T'_{\text{in}} - T_{\text{out}}) \tag{12}$$

$$\Delta T_{\min} = \min(T'_{\text{out}} - T_{\text{in}}, T'_{\text{in}} - T_{\text{out}}) \tag{13}$$

$$D_h = \frac{4A_c}{P} \tag{14}$$

The friction factor (f) is defined as

$$f = \frac{A_c}{A_0} \cdot \frac{2\Delta P}{\rho_f (u_{\max})^2} \tag{15}$$

where, A_c is the minimum free-flow area; u_{max} is the maximum velocity.

4.2 Model Validation. Prior to presenting the simulation results, it is important to validate the computational model. In order to compare the simulation results of the louver fin with the experimental results [8], which were obtained under the cross flow condition, the water zone in the simulation is assumed to be at a constant temperature. The comparison between the simulation and the experimental results is shown in Table 3. The deviation of the $StPr^{2/3}$ between the simulations by the RNG k-ε turbulence model and the experimental data are less than 5.4%, and the deviation of the friction factor f between the simulation and the experimental results less than 4.1%. Thus, there is a good agreement between the simulation and the experiment, in terms of thermal performance and the pressure loss.

4.3 Performance Comparison Among Three Configurations of HEX. The thermal performance and the pressure loss are two important factors in the heat exchanger design. In order to develop a high performance countercurrent flow HEX, three different configurations of fins (louver-, wavy-, and pin fin) are simulated. The thermal performance and the pressure loss are obtained by using ANSYS FLUENT.

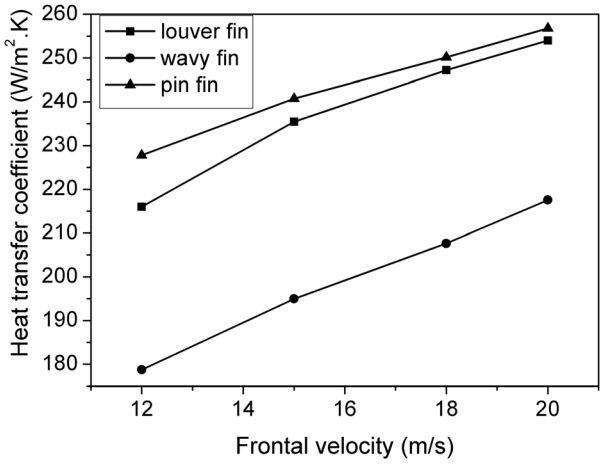

Fig. 4 Heat transfer coefficient versus frontal velocity

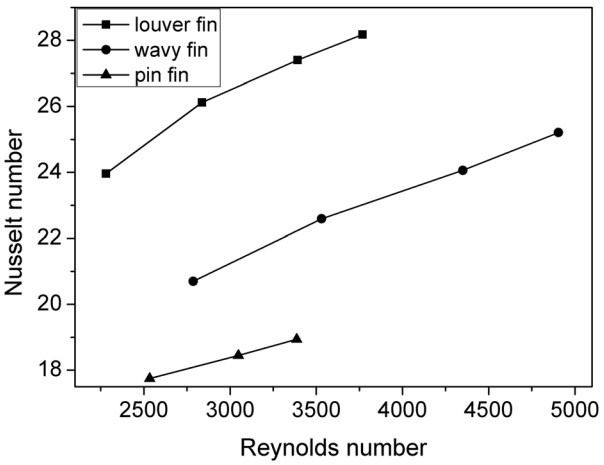

Fig. 5 Nusselt number versus Reynolds number

4.3.1 Thermal Performance. The heat transfer coefficients predicted for three configurations of fins are correlated with the frontal velocity, as shown in Fig. 4. Among these three configurations of fins, the cases with louver and pin fins reach higher heat transfer coefficients than does the wavy fin. The main reason causing the different heat transfer coefficients is probably the thermal boundary layers on the different configurations of the fins. For the louver fin, the boundary layer is developed along the louver, but it is broken at the end of the fin. The boundary layer cannot become thick due to the short louver length. This relatively thin boundary layer on the louver fin is the major factor to produce the high thermal performance. In addition, because the boundary layer separates around the pin fin, a high thermal performance is achieved as well. However, the thickness of the boundary layer on the wavy fin is kept constant, because the thickness is reduced on one side and increased on the other side at the same location. Due to the constant thickness boundary layer, the thermal performance of the wavy fin is not as good as that of the louver fin and the pin fin.

On the other hand, in order to remove the effect of different size of fin, the dimensionless parameters (Nu number and Re number) are introduced to analyze the thermal performance. Figure 5 illuminates the relationship between the Nu number and the Re number. The louver fin presents higher Nu number than do

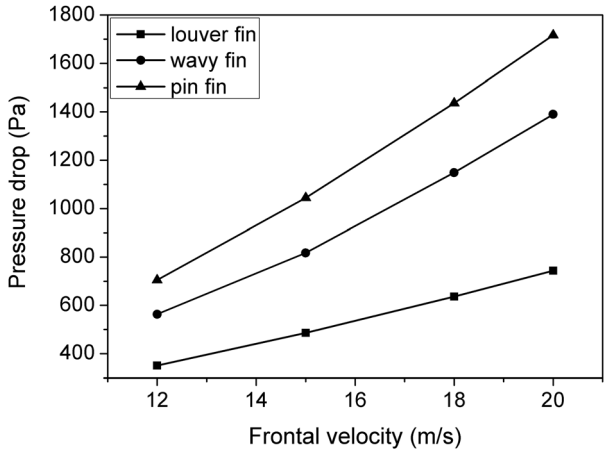

Fig. 6 Pressure drop versus frontal velocity

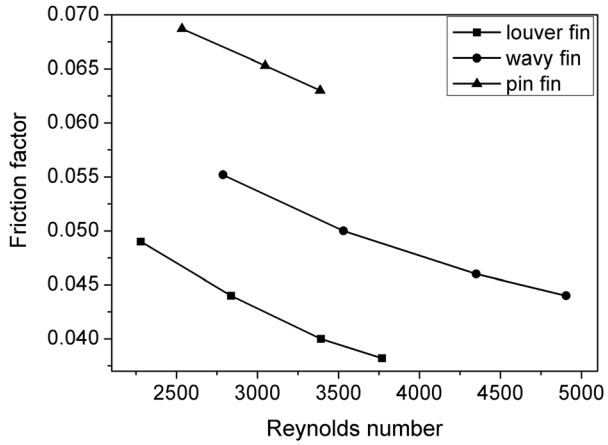

Fig. 7 Friction factor versus Reynolds number

the wavy fin and the pin fin at the same Re number. Even though the heat transfer coefficient is similar between the pin fin and the louver fin, due to the in-line fin pattern and the small hydraulic diameter in the pin fin, the Nu number is much lower in the pin fin than the one in the louver fin. Based on Figs. 4 and 5, it is revealed that the louver fin presents better thermal performance than the other cases.

4.3.2 Pressure Loss. Figure 6 illuminates the pressure drop through the three configurations of fins (louver-, wavy-, and pin fin) as a function of frontal air velocity. As expected, the pressure drops increase with increasing air velocity. The louver fin presents the lowest pressure drop among the three configurations. This result might appear because the flow through the louver fins becomes parallel to the louvers at high speed. In this case, the louver fins act like a flat plate, and the air flow path is smooth due to similarity with a "flat plate" boundary layer flow. However, the flow path might change its direction along the fins due to the structure of the wavy fin and pin fin. The smooth flow path along the louver fin might be the main reason causing the flow resistance in the louver fin to be lower than those of the wavy fin and the pin fin. The low flow resistance on the louver fin is also shown in Fig. 7. By considering the dimensionless parameter–friction factor (f), the louver fin has lower friction factor than the one in the wavy fin or the pin fin at the same Reynolds number.

4.4 Performance Comparison Between a Countercurrent Flow HEX and a Cross Flow HEX. Based on the analysis of thermal performance and pressure loss among the louver-, wavy-, and pin fins, it is proved that the louver fin presents higher thermal

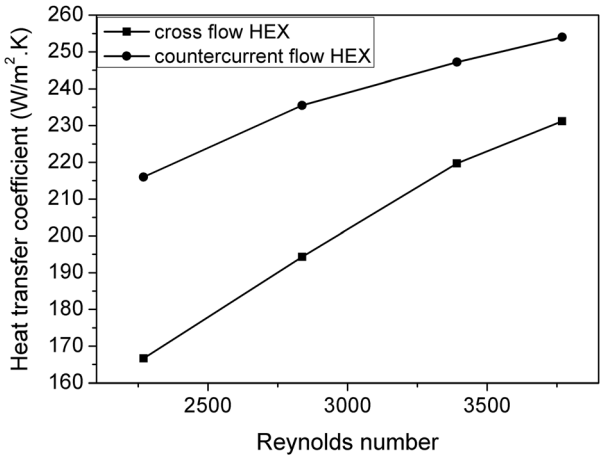

Fig. 8 Heat transfer coefficient in cross flow HEX and in countercurrent flow HEX

Table 4 Assumed operating data of a truck

Cooling power (kW)	200	
Truck speed (km/h)	65	
Radiator (water side)	$T_{in} = 90$ °C	$T_{out} = 85$ °C
Radiator (air side)	$T_{in} = 30$ °C	$T_{out} = 55$ °C

performance and lower pressure drop than do the wavy fin and the pin fin. Thus, the louver fin is chosen as the configuration of fin on the air side for the countercurrent flow HEX. In order to evaluate the performance of the countercurrent flow HEX, a conventional aluminum louver fin cross flow HEX is adopted for comparison. Due to the fact that the same louver fin is used in the countercurrent and cross flow HEXs, the flow resistance on the air side is the same for both cases. Thus, the pressure loss is not considered here.

The thermal performance comparison between the cross flow HEX and the countercurrent flow HEX is shown in Fig. 8. The countercurrent flow HEX has higher heat transfer coefficient than does the cross flow HEX. This result is mainly because the countercurrent flow arrangement could maximize the temperature difference between two fluids to transfer more heat than does the cross flow arrangement. When the Reynolds number varies from 2800 to 3800, the heat transfer coefficient of the countercurrent flow HEX is 21% to 9.8%, respectively, higher than the one in the cross flow HEX. This high heat transfer coefficient is beneficial to reduce the size of the countercurrent flow HEX compared to the cross flow HEX.

Furthermore, a specific case study (a typical truck with 200 kW cooling power) is carried out to analyze the performance of the countercurrent flow HEX. The operating data are shown in Table 4.

Based on this specific case, the different results between the countercurrent flow and the cross flow HEXs are shown in Table 5. Due to the high heat transfer coefficient performance in the countercurrent flow HEX, the total cooling surface area (air side) is reduced by 11.2% compared to the cross flow HEX. The overall size of the cross flow HEX could be designed as $1000 \times 337 \times 70$ mm (W × H × L). Meanwhile, the overall size of the countercurrent flow HEX could be designed as $1000 \times 300 \times 70$ mm (W × H × L). Because the cross-section area of the countercurrent flow HEX (1000 mm × 300 mm) is 11% less than that of the cross flow HEX (1000 mm × 337 mm), there is 11% reduction in power for pushing air through the countercurrent flow HEX.

However, due to the height of countercurrent flow HEX (300 mm), the streamline of flow field of the heavy vehicle might be destroyed, and a huge flow resistance might be presented to the vehicle. In order to reduce the flow resistance and optimize the performance of the countercurrent flow HEX, the countercurrent flow HEX

Table 5 Comparison between the cross flow HEX and the countercurrent flow HEX

	Cross flow HEX	Countercurrent flow HEX
Air side cooling surface area (m^2)	19.3	17.1 (11.2% reduction)
Overall size (W × H × L) (mm × mm × mm)	1000 × 337 × 70	1000 × 300 × 70
Total volume (m^3)	0.0236	0.021 (11% reduction)
Power for pushing air through HEX (W)	3858	3434 (11% reduction)

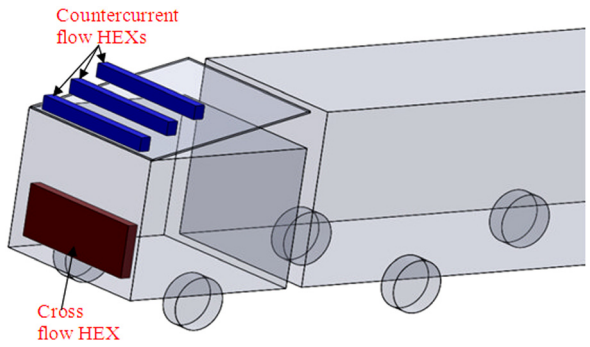

Fig. 9 Countercurrent flow HEX and cross flow HEX in a heavy duty truck

(1000 × 300 × 70 mm) is divided into three smaller countercurrent flow HEXs (the size of each one is 1000 × 100 × 70 mm). These three countercurrent flow HEXs are placed on the gradient roof of vehicle as like a staircase, as shown in Fig. 9.

After the analysis of the specific cases, several advantages and disadvantages of countercurrent flow HEX could be summarized as follows:

- Advantages:
  (1) The heat transfer coefficient is higher in the countercurrent flow HEX than the one in the cross flow HEX.
  (2) The overall size of the countercurrent flow HEX is smaller than that of the cross flow HEX, when the removed heat is the same.
  (3) The pressure loss is lower in the countercurrent flow HEX than the one in the cross flow HEX, because of the reduction of size in the countercurrent flow HEX.
  (4) The high heat transfer coefficient and low pressure loss lead to a high coefficient of performance in the countercurrent flow HEX.
- Disadvantages:
  1. The countercurrent flow HEX placed on the roof of the vehicle might destroy the streamline flow field of the vehicle. The collocation of countercurrent flow HEX should be optimized.
  2. The cooling air through the countercurrent flow HEX is driven by the movement of vehicles. When the vehicle climbs on a mountain, the speed of the vehicle is low. However, the engine cooling power is high at the same time. Thus, this problem should be analyzed in future work.

5 Conclusion and Recommendation

Due to the increasing cooling power and the space limitation in vehicles, it is impossible to increase the size of the radiator to dissipate the increasing amount of heat from the engine. Placing the radiator at the underbody of the vehicle or on the roof of the driver compartment might be a good method to handle the increasing cooling power. In this paper, a radiator is designed to be placed on the roof of the truck compartment. Due to the radiator position change, a countercurrent flow heat exchanger is accordingly proposed. The major results are as follows:

1. Compared to the wavy and the pin fins, the louver fin design presents high thermal performance and low pressure drop in the countercurrent flow HEX.
2. The heat transfer coefficient in the louver fin countercurrent flow HEX is 21%–9.8% higher than the one in the louver fin cross flow HEX when Reynolds number varies between 2800 and 3800.
3. For the specific case in this paper, the total cooling surface area of the countercurrent flow HEX could be reduced by 11.2% compared to the cross flow HEX. Moreover, the power for pushing air through the countercurrent flow HEX is 11% lower than that of the cross flow HEX.

Thus, placing a countercurrent flow HEX on the roof of the truck driver compartment is a useful method to dissipate the increasing cooling power in vehicles. However, there are still several problems facing the application of countercurrent flow HEX in vehicles. Thus, much effort (the collocation of HEX, air supply to HEX without fans, or the available place for a fan) has to be conducted for the development of countercurrent flow HEXs in vehicles.

Acknowledgment

The authors acknowledge the financial support from the Swedish Energy Agency and Volvo 3P.

Nomenclature

A_c = minimum free-flow area on the air side, m^2
A_0 = total heat transfer surface area on the air side, m^2
c_p = air specific heat, $J \cdot kg^{-1} \cdot K^{-1}$
D_h = hydraulic diameter, m
f = Fanning friction factor, dimensionless
h = heat transfer coefficient, $W \cdot m^{-2} \cdot K^{-1}$
H = height of fin, m
k = turbulent kinetic energy, $m^2 \cdot s^{-2}$
L = length of fin, m
m = air mass flow, $kg \cdot s^{-1}$
Nu = Nusselt number, dimensionless
P = wetted perimeter of passages on the air side, m
P_k = production of turbulent kinetic energy
Pr = Prandtl number, dimensionless
Q = total amount of heat dissipating to air side, W
Re = Reynolds number, dimensionless
St = Stanton number, dimensionless
T_{in} = air inlet temperature, K
T_{out} = air outlet temperature, K
T'_{in} = water inlet temperature, K
T'_{out} = water outlet temperature, K
u = air velocity, $m \cdot s^{-1}$
W = width of fin, m
ΔP = pressure drop through fins, Pa
ΔT = logarithmic mean temperature difference, K
ε = rate of energy dissipation
λ = thermal conductivity, $W \cdot m^{-1} \cdot K^{-1}$
ρ = density of fluid, $kg \cdot m^{-3}$
μ = dynamic viscosity of air, Pa s

Subscripts

f = air fluid
max = maximum
min = minimum
t = turbulent

References

[1] Hountalas, D. T., Mavropoulos, G. C., and Binder, K. B., 2008, "Effect of Exhaust Gas Recirculation (EGR) Temperature for Various EGR Rates on Heavy Duty DI Diesel Engine Performance and Emissions," Energy, **33**, pp. 272–283.

[2] Doughty, D. H., Butler, P. C., Jungst, R. G., and Roth, E. P., 2002, "Lithium Battery Thermal Models," J. Power Sources, **110**, pp. 357–363.

[3] Khaled, M., Harambat, F., and Peerhossaini, H., 2010, "Underhood Thermal Management: Temperature and Heat Flux Measurements and Physical Analysis," Appl. Therm. Eng., **30**, pp. 590–598.

[4] Larsson, L., Wiklund, T., and Löfdahl, L., 2011, "Cooling Performance Investigation of a Rear Mounted Cooling Package for Heavy Vehicles," SAE Technical Paper No. 2011-01-0174.

[5] Malvicino, C., Mattiello, F., and Seccardini, R., 2011, "Flat Heat Exchangers," Proceedings of the 10th Vehicle Thermal Management Systems Conference and Exhibition, Gaydon, Warwickshire, UK, pp. 91–98.

[6] Malvicino, C., Sciullo, F. D., Cuniberti, M., Vestrelli, F., and Beltramelli, F., 2011, "Dual Level Vehicle Heat Rejection System," Proceedings of the 10th Vehicle Thermal Management Systems Conference & Exhibition, Gaydon, Warwickshire, UK, pp. 473–480.

[7] Shah, R. K., and Sekulic, D. P., 2003, *Fundamentals of Heat Exchanger Design*, John Wiley & Sons, New York.

[8] Kays, W. M., and London, A. L., 1995, *Compact Heat Exchangers*, 3rd ed., McGraw-Hill, New York.

[9] Pope, S. B., 2000, *Turbulent Flows*, Cambridge University, Cambridge, England.

[10] ANSYS, Inc., 2009, ANSYS FLUENT 12.0—Theory Guide.

[11] Tannehill, J. C., Anderson, D. A., and Pletcher, R. H., 1997, *Computational Fluid Mechanics and Heat Transfer*, 2nd ed., Taylor & Francis, London.

[12] Versteeg, H. K., and Malalasekera, W., 2007, *An Introduction to Computational Fluid Dynamics*, 2nd ed., Pearson Prentice-Hall, Englewood Cliffs, NJ.